Article:
Arabskyj, Luke, Qiao, Liang, Permogorov, Dmitri et al. (2025) Characterisation of a Low-Noise Tuneable Silicon Single-Photon Avalanche Diode. Journal of lightwave technology. pp. 1815-1821. ISSN: 0733-8724

https://doi.org/10.1109/JLT.2025.3646065

Characterisation of a Low-Noise Tuneable Silicon Single-Photon Avalanche Diode

Luke Arabskyj, Liang Qiao, Dmitri Permogorov, Marco Lucamarini, and Christopher Chunnilall

***Abstract*—Silicon single-photon avalanche diodes (Si-SPADs) are widely used in lightwave applications such as quantum communication, medical imaging, time-of-flight systems and quantum optical metrology, due to their sensitivity, accuracy, compactness and cost-effectiveness. The most important performance metric depends on its intended application. Each metric has a dependence on operating parameters such as bias voltage and operating temperature. Some metrics, e.g. detection efficiency and timing precision, exhibit performance trade-offs with noise. However, plug-and-play Si-SPADs typically have fixed bias voltage and operating temperature, which significantly limits user control, adaptability, and performance. In this study, a recently developed commercially available free-space Si-SPAD with adjustable bias voltage, temperature control, an integrated frequency counter and a large sensing area was evaluated. Key performance metrics were traceably measured as functions of bias voltage and temperature, including dark count rate, dead time, timing precision, afterpulse probability and photon detection efficiency at 852 nm. Results are benchmarked against existing reports of other commercially available Si-SPAD detectors. Notable strengths include low dark count rates (4 to 10 s^{-1}), a large sensing area (diameter = 500 μm), and high timing precision (163 to 212 ps), whilst maintaining a detection efficiency greater than 40%. These characteristics make the detector a strong candidate for deployment across a range of applications, particularly those operating outside of lab conditions where operational flexibility is essential.**

***Index Terms*—Quantum information, quantum metrology, Si-SPAD, single-photon avalanche diodes, single-photon detectors.**

Received 30 July 2025; revised 11 December 2025; accepted 15 December 2025. Date of publication 19 December 2025; date of current version 2 March 2026. This work was supported in part by the National Physical Laboratory (NPL) Measurement for Quantum (M4Q) programme and in part by the EPSRC Integrated Quantum Networks (IQN) Research Hub under Grant EP/Z533208/1, both are funded by the U.K. Government Department for Science, Innovation and Technology through the U.K. National Quantum Technologies Programme. *(Corresponding author: Luke Arabskyj.)*

Luke Arabskyj is with the National Physical Laboratory, Teddington TW11 0LW, U.K., and also with the School of Physics, Engineering & Technology and York Centre for Quantum Technologies, University of York, York YO10 5FT, U.K. (e-mail: luke.arabskyj@npl.co.uk).

Liang Qiao and Dmitri Permogorov are with RedWave Labs, Harwell Innovation Centre, OX11 0QG Didcot, U.K.

Marco Lucamarini is with the School of Physics, Engineering & Technology and York Centre for Quantum Technologies, University of York, York YO10 5FT, U.K.

Christopher Chunnilall is with the National Physical Laboratory, Teddington TW11 0LW, U.K.

Color versions of one or more figures in this article are available at https://doi.org/10.1109/JLT.2025.3646065.

Digital Object Identifier 10.1109/JLT.2025.3646065

I. Introduction

SINGLE-PHOTON avalanche diodes (SPADs) are compact semiconductor devices capable of detecting individual photons with high accuracy and efficiency. Their sensitivity is achieved by reverse biasing a p-n junction above its breakdown voltage (V_{bd}). In this regime, the depletion region is extended, and a strong electric field is established. When an incident photon generates an electron-hole pair in the active region, the resulting free charge carrier is rapidly accelerated by the field. With sufficient momentum, the carrier triggers impact ionisation, creating a charge avalanche which increases exponentially. Due to this ability to turn the absorption of a photon into a measurable current, SPADs are widely used across a range of applications, including biomedical imaging [1], [2], light detection and ranging (LiDAR) [3], [4], quantum communication [5], [6], and other quantum technologies such as quantum random number generation [7]. They also play a critical role in validating traceability to primary optical standards in the few-photon regime [8], [9], making them of significant interest to the field of metrology [10], [11], [12], [13], [14], [15].

A SPAD's performance metrics include dark count rate (DCR), dead time (τ) and recovery time, afterpulse probability (APP), timing precision or jitter, and detection efficiency (DE) [16]. Each is influenced to varying degrees by the reverse bias voltage (V_{bias}) and the operating temperature [17]. A specific metric may be optimised through adjustment of these two parameters. However, optimisation of one can lead to the degradation of another, resulting in performance trade-offs [18]. For example, increasing V_{bias} enhances the DE and timing precision, but it also increases the DCR and APP. Although enhancing DE and timing precision can be advantageous, in some applications—for example, long-range quantum key distribution (QKD)—detector noise can be the primary limiting factor [19]. These points highlight the need for V_{bias} and thermoelectric temperature (T_{TEC}) control. Currently, both parameters are fixed during the assembly process of all packaged plug-and-play Si-SPADs.

The performance of the AD200 Si-SPAD recently developed by RedWave Labs (RW) has been characterised. It integrates internally developed electronics with commercially available Si-SPAD sensors to create user-configurable plug-and-play detectors with V_{bias} and T_{TEC} control. An internal frequency counter with a variable time window is included, enhancing its functionality whilst maintaining a compact footprint. The commercial sensors which RW integrate with their electronics

are Laser Components' SAP500-Series avalanche photodiodes (APDs). These are large area sensors (diameter = 500 μm) reported to have excellent timing precision and enhanced photon absorption in the near-infrared (NIR) resulting from their back-illuminated reach-through design [20], but are unavailable as packaged plug-and-play detectors. These points mark the AD200 as a versatile tool for a wide range of applications, including research in the field of quantum communications, where they have already been successfully deployed [21], [22].

II. Performance Characterisation

The AD200's performance was characterised at six bias voltages, $V_{\text{bias}} = \{112\text{\textbackslash,V}, 113\text{\textbackslash,V}, 114\text{\textbackslash,V},..., 117\text{\textbackslash, V}\}$, each tested at three temperature settings: $T_{\text{TEC}} = \{$-25°C; -20°C; -15°C$\}$, yielding 18 distinct operating conditions per metric. The maximum bias voltage of 117V was recommended by RW for this specific device; whereas the temperatures were selected to enable a fair comparison with similar commercially available Si-SPADs, which are typically operated at –20°C. Tuneability of these parameters is enabled by USB connection and a graphical user interface; alternatively, serial commands can be used to read and write.

Conventionally, V_{bias} is expressed relative to V_{bd} as over voltage (V_{ov}), where $V_{\text{ov}} = V_{\text{bias}}$ - V_{bd}. This is because V_{bd} provides a clear point of reference at which single-photon sensitivity is achieved. However, because V_{bd} was not provided by RW, it was estimated by illuminating the device with approximately 1000 incident photons per second whilst scanning V_{bias} and monitoring the detector clicks. It was assumed that the bias voltage at which detection events began was equivalent to V_{bd}. Although this approach is commonly used [20], [23], it is inaccurate; furthermore, V_{bd} changes with temperature. Therefore, each metric is presented as a function of both V_{bias} and V_{ov} to provide a comprehensive overview of the performance characteristics available to a user.

A. Dark Count Rate

A dark count is the result of an avalanche which occurred in the absence of incident light [24]. These discrete events follow a Poisson distribution and mark the intrinsic noise floor of a detector. Dark counts can be divided into two contributing groups [25]: primary contributors are a combination of thermal excitations and band-to-band tunnelling, with the latter accounting for a smaller fraction [26]; secondary contributors are afterpulses, which are evaluated in Section II-D.

To measure the AD200's DCR, the device was sealed in a light-tight enclosure with a cap placed over the sensor. Detection events were recorded with a FAST ComTec MCS6A, a time-correlated single-photon counter (TCSPC) with a resolution of 100 ps and no deadtime. Fig. 1(a) illustrates the DCR probability density, measured with $V_{\text{bias}} = 117$V and $T_{\text{TEC}} =$ -20 °C over approximately 24 hours. Included within Fig. 1(a) is the Poisson distribution corresponding to the arithmetic mean obtained from the experimental data. A chi-squared test yielded $\chi^2 = 0.0006$ with 21 degrees of freedom (p ≈ 1.000), indicating excellent agreement with the Poissonian model.

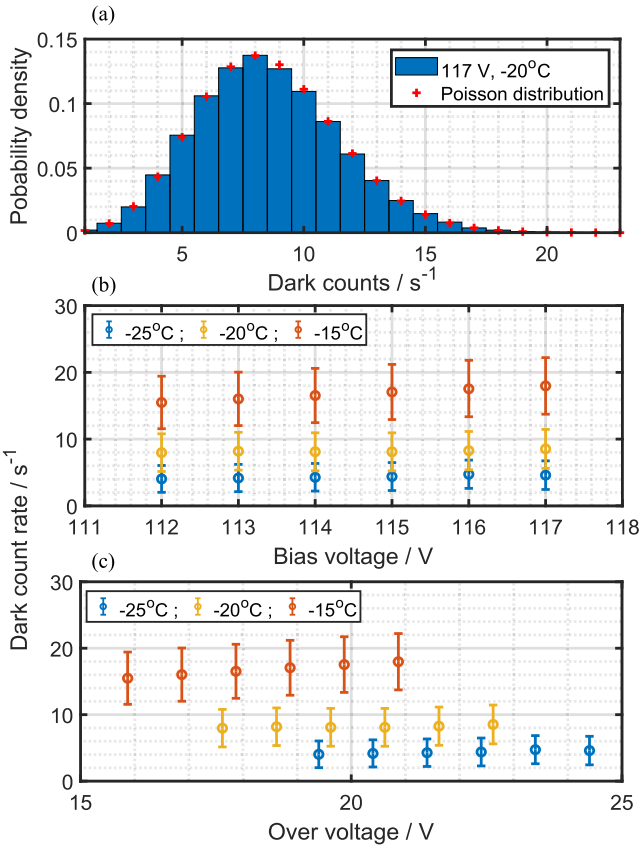

Fig. 1. (a) Dark count rate (DCR) probability density recorded with $V_{\text{bias}} =$ 117 V and $T_{\text{TEC}} = -20$ °C. (b) Mean DCRs as functions of bias voltage and temperature. (c) Same data as in (b), but plotted as a function of over voltage.

Fig. 1(b) and (c) display the DCR results as functions of V_{bias} and V_{ov}, respectively. Error bars indicate the standard deviations of events. Previous work on a SAP500 series APD identified a positive parabolic dependence on V_{ov} [20]; however, parabolas with both positive gradients and y-intercepts at the origin ($V_{\text{ov}} =$ 0, DCR = 0) are not consistent with these results. The increase in DCR with voltage is marginal, indicating that dark counts originating from band-to-band tunneling are negligible [18]. In contrast, cooling the detector has a significant effect on the noise, suggesting trap-assisted thermal excitations are the dominant mechanism. Considering the large area of the sensor, and the correlation between DCR and depletion region volume [27], the measured DCRs are notably low, surpassing values previously reported with the same sensor model [20], [22].

B. Dead Time

Dead time (τ) refers to the period of time in which the detector is incapable of producing a measurable output signal despite the absorption of a photon [24]. It is a result of the quenching mechanism, used to suppress an avalanche, that prepares the detector for the next detection. Quenching is achieved by applying a voltage which temporarily drops V_{bias} to a value below V_{bd}. Because each detector event incurs a dead time, it imposes a maximum detection rate of $1/\tau$. It also provides time for carriers trapped by impurities/defects during an avalanche to be

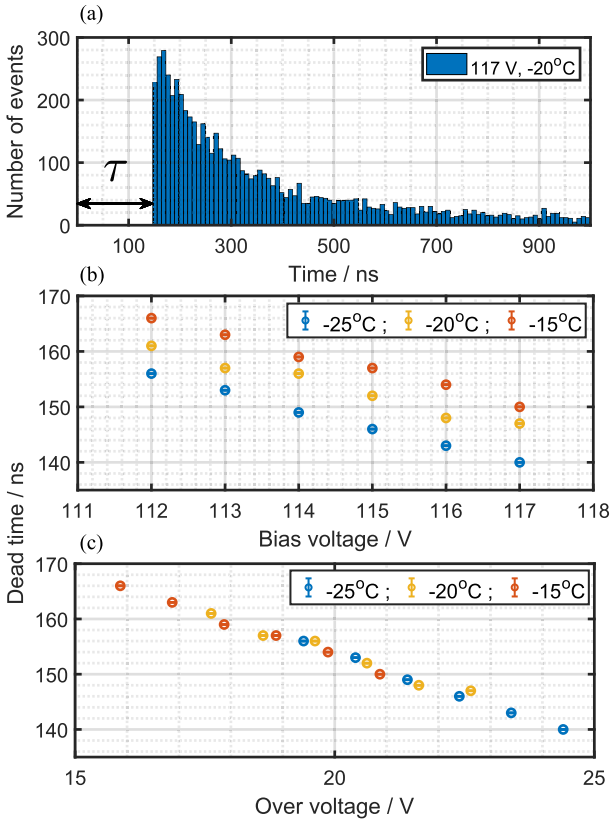

Fig. 2. (a) A histogram of the time between neighbouring dark counts measured at $V_{\text{bias}} = 117$ V and $T_{\text{TEC}} = -20\,^{\circ}$C, τ marks the dead time. (b) Dead times plotted as a function of bias voltage. (c) Same data as in (b) but plotted as a function of over voltage. Due to the sparsity of events, histogram bin widths were increased in (a) for clarity; however, the maximum resolution of 100 ps was used for data presented in (b) and (c). Error bars are present but not visible, with magnitudes of $\pm$ 300 ps.

released, which may otherwise initiate a subsequent avalanche in a process known as afterpulsing. This presents a trade-off between the maximum achievable count rate and afterpulsing: most commercially available Si-SPADs operate with a dead time between 20 and 50 ns. However, dead times as low as 4 ns have been achieved whilst maintaining an afterpulse probability less than 2% [28]. Fig. 2(a) displays a histogram of the time between neighboring dark count events. The minimum time difference, marked by τ, quantifies the dead time. Fig. 2(b) and (c) display the results as functions of V_{bias} and V_{ov}, respectively.

The temperature dependence observed in Fig. 2(b) is a result of the V_{bd} changing with temperature, which becomes clear when evaluating the data as a function of V_{ov} (Fig. 2(c)). The voltage dependence stems from the shorter time during which the voltage remains below V_{bd} after quenching (see Fig. 1 in [29]), thereby reducing the detector's dead time. With τ values ranging between $\approx$140 and 165 ns, the AD200 has a dead time an order of magnitude longer than most competing devices which will compromise its use in high detection rate applications.

C. Timing Jitter

Timing jitter is the variation in time between the arrival of a photon and the corresponding output detection signal [24]. This variation, or jitter, has two characteristic components, a peak and a diffusion tail [30]. The peak is correlated to carriers generated within the depletion region, whereas the diffusion tail is a result of carriers generated in the neutral regions which must first migrate to the depletion region before impact-ionisation can occur. Due to the statistical nature of the physical processes at work (see [18] for an overview) the full-width at half-maximum (FWHM) of a Gaussian distribution is generally used to quantify the jitter; however, it does not accurately model the diffusion tail.

Detector jitter may be minimised by illuminating the sensor centrally [31], [32] with a narrow beam waist [33], [34]. Therefore, to characterise the AD200's timing-response a centrally aligned 20 μm beam consisting of weak optical pulses was used. The pulsed source was a mode-locked Ti:Sapphire laser, tuned to 852 nm, with 14 ps duration pulses at a repetition rate of 80 MHz. The laser was attenuated such that each pulse contained, on average, approximately 0.003 photons, which corresponded to 10^5 detector clicks per second. A Hydra Harp 400 TCSPC was used to correlate detection events with incident laser pulses with 8 ps resolution; a Gaussian distribution was fitted to the data to obtain the FWHM. Fig. 3(a) displays the detector jitter at $V_{\text{bias}} = 117$ V and $T_{\text{TEC}} = -20\,^{\circ}$C.

Figs. 3(b) & 3(c) display the range of tested voltages and temperatures; all fits had an R-squared value > 0.99. With jitter values ranging between $\approx$160 to 220 ps, the AD200 has a timing precision comparable to or better than competing detectors (see Section III, Table I), which may be attributed to the relatively short conversion region of the sensor. Generally, reducing the conversion region impacts the quantum efficiency of the device at longer wavelengths; however, the use of a rear metal oxide layer behind the p-n junction acts as a mirror, effectively doubling the photon conversion path, without increasing the distance a free charge carrier must first migrate before triggering an avalanche. In turn, this improves the DE whilst maintaining a respectable timing response [29]. The decrease in jitter with respect to voltage is linked to a proportional rise in electric field strength, leading to an increase in the average kinetic energy of avalanching electrons. This translates into an increase in avalanche propagation speed, thereby enhancing the timing response [32]. As was the case with dead time, the apparent temperature dependence of Fig. 3(b) is predominantly a result of the shifting V_{bd}, which is apparent from Fig. 3(c).

1) Count Rate Dependence: The correlation between timing jitter and count rate is widely recognised [35]; it has the potential to be problematic for applications like time-bin encoded quantum key distribution (QKD), where both high detection rates and accurate timing are paramount [36]. Count rate dependence generally becomes non-negligible for rates greater than 10^5 per second and is largely due to the pulse-processing electronics [35]. For example, the imperfect settling of V_{bias} between detection events can play a significant role as the rate increases [29]. To test the AD200's count rate dependence, the detector's jitter was measured as described above, whilst the device registered 50 k cps, 100 k cps and 500 k cps with $V_{bias} = 117$ V and $T = -20$°C. These three count rates corresponded to, on average, approximately 0.0014, 0.0028 and 0.014 photons per pulse, respectively. Fig. 4 shows the results with the y-axis scaled logarithmically.

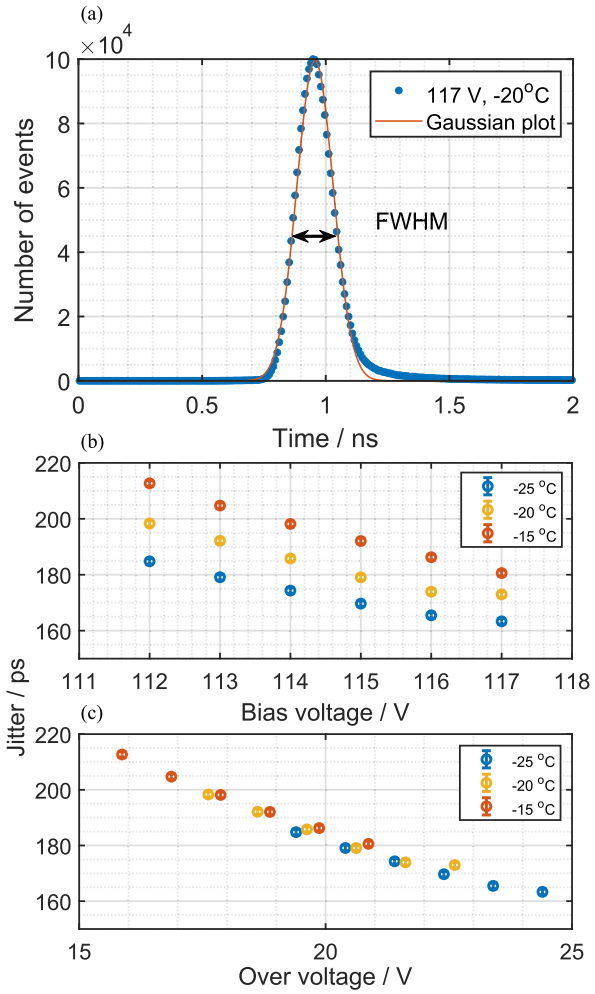

Fig. 3. (a) Timing response histogram measured at $V_{\text{bias}} = 117$ V and $T = -20°$C. (b) Timing response FWHM values plotted as a function of bias voltage. (c) Same data as in (b) but plotted against over voltage. Uncertainties were taken from each Gaussian fit.

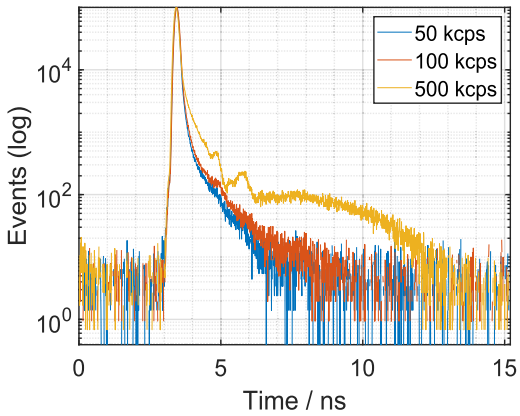

Fig. 4. The AD200's timing response characterised at three count rates.

The FWHMs of the fitted Gaussian functions were found to increase with count rate, with values of 170.0(6) ps, 173.0(6) ps and 178(1) ps for the 50 kcps, 100 kcps and 500 kcps rates, respectively. However, it is clear that the FWHM alone is not a good metric for quantifying the change in response. To address this, the total duration of each response as well as the weighting of all events after the Gaussian peak with respect to those before were evaluated. The total durations in ascending count rate order were found to be approximately 5.7 ns, 6.7 ns and 10.3 ns. Similarly, the weighting of events after the peak with respect to those before increased significantly, with values of approximately 1.18, 1.28 and 1.41. The additional features present in the diffusion tail of the 500 kcps dataset are of unknown origin but were verified as a property of the detector and not the setup by testing other commercially-available detectors under identical conditions.

D. Afterpulse Probability

Once an avalanche is triggered, charge carriers can become trapped by charged defect states due to imperfections in the semiconductor. Once the quenching mechanism has reset the detector, the trapped carriers can be released, potentially triggering a subsequent avalanche in a process known as afterpulsing. These correlated events are a source of detector noise which typically contribute a few percent of the total clicks in Si-SPADs. The setup used to quantify the AD200's APP utilised a time-correlated pulsed laser method, similar to that described by Dejen et al. [11]. A laser diode with a centroid wavelength of 852 nm was driven by an arbitrary waveform generator (AWG) such that optical pulses lasting 4 ns in duration were incident upon the detector at a frequency of 100 kHz. A relatively low frequency ensures that the probability of an afterpulse is negligible by the time the next optical pulse arrives; 4 ns pulses were chosen to minimise their duration whilst remaining above the laser's modulation bandwidth. A FAST ComTec MCS6A TCSPC was used to correlate detection events with the incident optical pulses using the AWG's synchronisation output signal. Fig. 5(a) displays a histogram of the correlated time differences. The total number of afterpulses per detection (n_{ap}) was quantified by the ratio of afterpulse detections to optical detections:

$$n_{\text{ap}} = \frac{\sum_{i=1} (N_{\text{ap},i} - \overline{B})}{\sum_{j=1} (N_{\text{optical},j} - \overline{B})}, \tag{1}$$

where $N_{\text{ap},i}$ is the number of afterpulse events in the i^{th} bin (black data within Fig. 5(a)), $N_{\text{optical},j}$ is the number of optical events in the j^{th} bin (red data within Fig. 5(a)) and $\overline{B}$ is the mean background value per bin (blue data within Fig. 5(a)). However, because n_{ap} contains higher order afterpulses, a correction is required which takes the form of a geometric series [11], [37]. Therefore, the APP (P_{AP}) for any given event is calculated by

$$P_{\text{AP}} = \frac{n_{\text{ap}}}{1 + n_{\text{ap}}}. \tag{2}$$

From Fig. 5(b) and (c), the APP's dependence on V_{bias} can be understood by the flow of charge during an avalanche (Q_{av}): an increase in Q_{av} corresponds to an increase in charge carriers, each with a finite probability of being trapped; because $Q_{\text{av}} \propto V_{\text{ov}}$, a linear relationship between the APP and V_{bias} is expected [38], [39]. Decreasing the temperature increases the APP due to the lifetime of defect states increasing as the temperature decreases. It is also clear that reducing the dead time increases

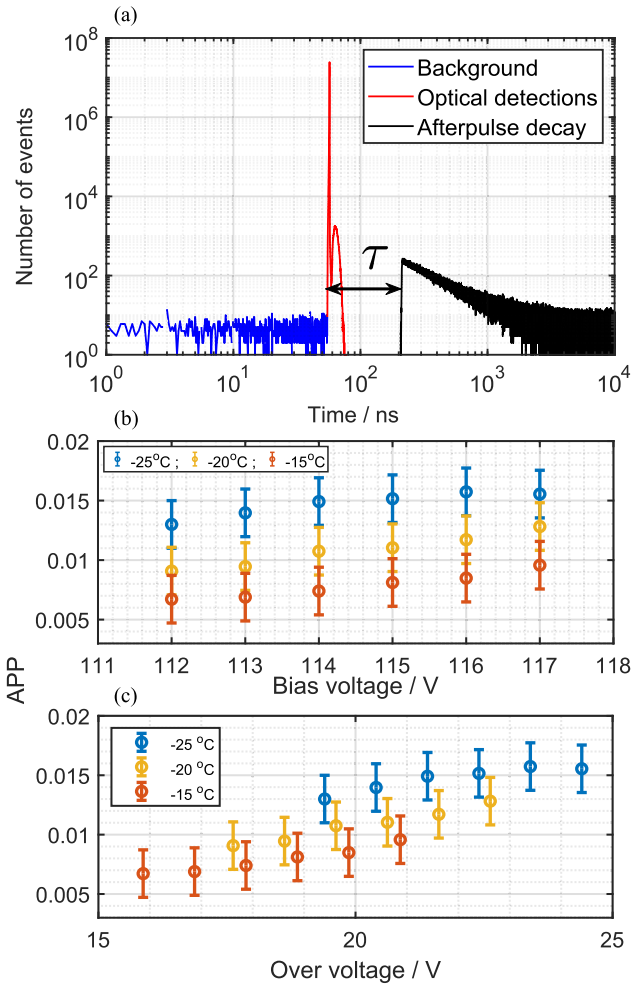

Fig. 5. (a) Histogram of detection events correlated with incident optical pulses. (b) Total APP plotted as a function of bias voltage, and (c) over voltage.

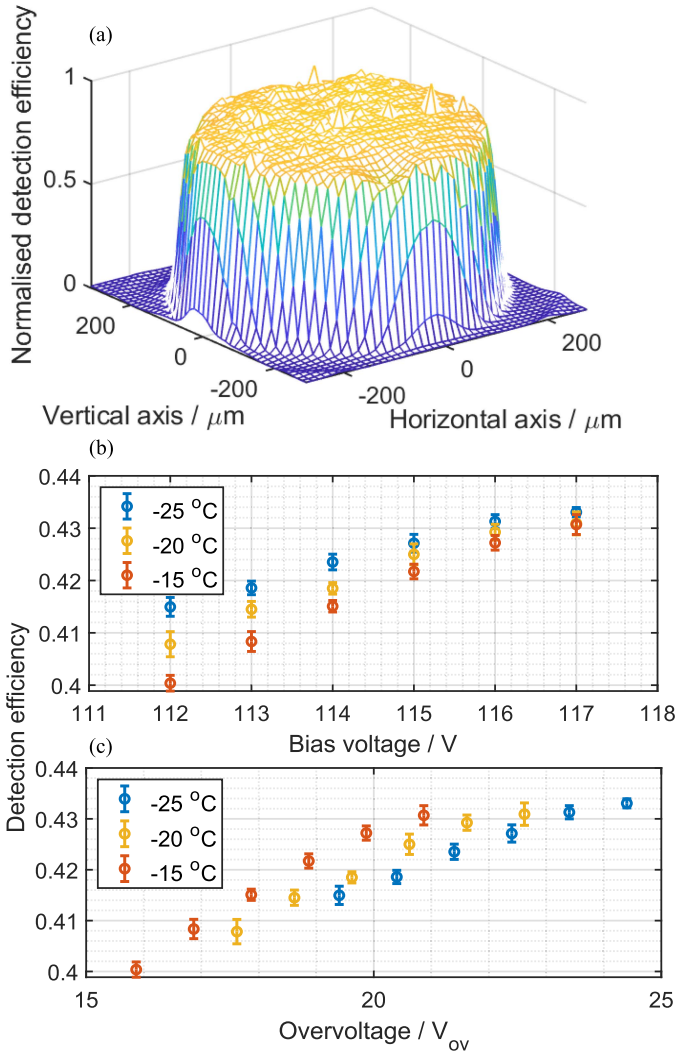

Fig. 6. (a) Spatial response map normalised to its maximum value; measurements were taken in 12.5 μm steps, with a horizontal position uncertainty of 0.2 μm (half the encoder resolution) per step and a negligible range uncertainty of 5 μm / 1m. For the vertical stage (without an encoder), Fig. 5 in [12] indicates a step uncertainty below 1.25 μm (half of a 2.5 μm step) due to the absence of fringe discontinuity; we assume the same 1.25 μm for the 12.5 μm step, with a negligible range uncertainty of 80 μm / 12 mm. (b) DE values presented as a function of bias voltage and (c) over voltage.

APP, highlighting the trade-off between maximum detection rate and APP.

Interestingly, a second peak is observed in Fig. 5(a) after the initial steep peak marking the rising edge of the optical pulses. This feature is not intrinsic to the 4 ns incident pulses, as confirmed by (a) testing multiple SPADs from other manufacturers under identical conditions and (b) observing no change when tilting the detector, ruling out reflections. At present, the origin of this peak is unknown.

E. Detection Efficiency

In most applications, DE is the critical metric. It is defined as the probability of an incident photon producing a measurable avalanche whilst the device is on and ready to detect [24]. In the ideal case, a detector's efficiency would be unity. However, losses due to reflections, the intrinsic quantum efficiency of the semiconductor, failed avalanches and other factors, all contribute to a non-unity DE [18]. To quantify the DE of the AD200, it was mounted on translation staging in the National Physical Laboratory's SI-traceable detector calibration facility [40]. A spatial response map was first measured with a focused 20 μm Gaussian beam produced by a continuous-wave laser diode operated at 852 nm (Fig. 6(a)). The beam was then aligned with the centre of the sensor, and the detector's response was recorded with a fixed incident mean photon number μ of $\approx 10^5$ per second for each temperature and voltage setting. The detection efficiency for each voltage and temperature, $\eta_{(V,T)}$, was then calculated by

$$\eta_{(V,T)} = \frac{N_{clicks} - N_{bg}}{\mu \cdot (1 - N_{clicks} \cdot \tau_{(V,T)})}(1 - P_{AP(V,T)}), \qquad (3)$$

where N_{clicks} are the average detection events per second, N_{bg} are the average number of background events, and $P_{\text{AP(V,T)}}$ and $\tau_{\text{(V,T)}}$ are the measured voltage and temperature dependent APP and deadtime values, presented in Sections II-D and II-B,

TABLE I
COMPARISON OF THE AD200 RESULTS WITH OTHER COMMERCIALLY-AVAILABLE SI-SPADS. DETECTION EFFICIENCY VALUES AT 852 NM WERE ESTIMATED FROM WAVELENGTH RESPONSE FIGURES AVAILABLE IN THE REFERENCED DATA SHEETS. FOR DETECTORS WITH MULTIPLE SENSOR AREAS AVAILABLE, THOSE CLOSEST IN DIAMETER TO THE SAP500 ARE PRESENTED.

Detector	Active area ⌀ / μm	DE @ 852 nm	DCR / s^{-1}	τ / ns	APP / %	Jitter (FWHM) / ps
RedWave AD200	500	0.40 to 0.44	4 to 18	140 to 166	0.6 to 1.5	163 to 212 (TTL)
Excelitas SPCM-AQRH [42], [43]	180	0.52	25 to 1500	22 to 42	0.5	225 to 350 (TTL)
Laser Components COUNT-NIR [44]	100	0.54	50 to 500	42 to 48	0.2	1000 (TTL)
MPD PDM [45]	100	0.11	<25 to <500	77	0.1 to 3.0	35 (NIM); <250 (TTL)
Hamamatsu C16531-100GD [46]	100	0.21	150	*Not specified*	0.1	*Not specified*

respectively. The (1 - $N_{\text{clicks}}\cdot\tau_{(\text{V,T})}$) term gives the fraction of time the detector was ready to detect and therefore corrects for photons lost within the deadtime. Results are presented in Fig. 6(b) and (c).

The relation between DE and V_{bias} can be understood by the electron/hole ionisation coefficients' dependence on electric field strength [41]. The temperature dependence is interesting to compare: for a given V_{bias}, the DE is shown to increase with a decrease in temperature; however, given a fixed over voltage, the opposite relation is true. This change in trend is a result of V_{bd} changing with temperature. Given that V_{bd} varies between devices, even when from the same sensor batch, this highlights the importance of referencing to V_{bd} rather than quoting an arbitrary V_{bias} value.

III. DISCUSSION

The results of the previous section show that the tuneability of the AD200 enhances the dynamic range of the device. For example, increasing the bias/over voltage improved both the DE and timing precision significantly, as shown in Figs. 6 and 3, respectively. The cost of these gains typically comes with an increase in noise [18], [20]. However, with measured DCRs ranging between 4 s^{-1} and 18 s^{-1}, low noise was maintained up to the maximum bias voltage. Considering the large sensing area of the SAP500 and the volume dependence of dark counts, DCRs of this magnitude are impressive, which the manufacturer attributes to its reach-through structure [47]. Similarly, noise originating from afterpulsing was low across the range of tested parameters; however, this was due to the detector's long deadtime effectively suppressing the APP. Previous work on a SAP500 sensor reported values greater than 4% with a dead time of 26 ns at $T_{\text{TEC}} = -20\,^{\circ}\text{C}$ [20]. Therefore, if the AD200's deadtime was reduced, thereby improving its maximum detection rate, the trade-off between DE and noise would be more prominent.

Table I compares the AD200's measured performance metrics with other commonly used commercially-available plug-and-play Si-SPADs. State-of-the-art performance is apparent in two areas - DCR and timing precision. The observed DCRs combined with DE values >40% at 852nm will be of significant interest in the field of long range QKD, where transmission distance is limited by detector noise [19]. In this application, operating the AD200 at the minimum temperature and maximum V_{ov} would be advantageous, as it reduces the DCR while maintaining high DE, thereby extending the potential transmission distance. For timing precision, the MPD detectors clearly outperform the others, but they do so at the cost of a significantly reduced DE. The AD200 maintains a respectable DE with a timing precision generally less than 200 ps. This will be of particular interest to applications requiring precise timing, such as time-of-flight applications as well as Bell-type measurements which address the locality loophole. For these applications, it would be beneficial to maximise DE and timing precision through V_{ov}, whilst minimising DCR via temperature control. Although reducing the operating temperature effectively lowers DCR, it also increases correlated noise due to afterpulsing. By implementing the AD200, these trade-offs can be systematically characterised and optimised for specific applications.

The detector's spatial response uniformity is also impressive, with other detectors often having a significant slope in response [14], [48]. This will be useful for free-space applications where the point of incidence of arriving photons can change with time. Another field anticipated to benefit from the observed uniformity is metrology in which a significant uncertainty contribution arises from uncertainty in an incident beam's position relative to the detector's non-uniform response [12], [14].

The primary drawback of the AD200 is its relatively long dead time. Ranging from 140 ns to 166 ns, the detector's maximum detection rate is reduced by a factor of approximately two to seven compared to those listed in Table I.

IV. CONCLUSION

Independent characterisation of RedWave lab's AD200 Si-SPAD detector was performed at multiple V_{bias} and T_{TEC} settings. Tuneability of these parameters enables device optimisation for a specific application and real-time adjustment. However, the commonly occurring trade-offs which are dependent on V_{bias}—specifically, DE and timing precision vs noise—were found to be minimal as a consequence of the detectors exceptionally low noise characteristics. Combining this with the intrinsic characteristics of the SAP500 sensor—e.g. a spatially uniform large sensing area and high timing precision—marks the AD200 a promising tool for many applications. It is particularly well suited for long range QKD, metrology and free-space applications where the spatial location of incident photons may change with time. However, with a deadtime of approximately 150 ns, the detector is currently not well-suited for applications requiring high detection rates and would benefit significantly from a reduction in this value. This improvement, however, would come at the cost of an increased after-pulse probability.

REFERENCES

[1] Y. Lin, P. Mos, A. Ardelean, C. Bruschini, and E. Charbon, "Coupling a recurrent neural network to SPAD TCSPC systems for real-time fluorescence lifetime imaging," *Sci. Rep.*, vol. 14, no. 1, pp. 1–13, 2024.

[2] M. G. Tanner, "Time resolved photon counting CMOS SPAD arrays for clinical imaging and spectroscopy," presented at the Eur. Conf. Biomed. Opt., Munich, Germany, Jun. 25–29, 2023, Paper 1262720.

[3] G. Chen, C. Wiede, and R. Kokozinski, "Data processing approaches on SPAD-based d-TOF LiDAR systems: A review," *IEEE Sensors J.*, vol. 21, no. 5, pp. 5656–5667, Mar. 2021.

[4] M. Chen, P. R. Rao, and E. Venialgo, "Depth estimation in SPAD-based LIDAR sensors," *Opt. Exp.*, vol. 32, no. 3, pp. 3006–3030, 2024.

[5] Y. Noblet and R. Donaldson, "BB84 quantum key distribution transmitter utilising broadband sources and a narrow spectral filter," *Opt. Exp.*, vol. 31, no. 9, pp. 15145–15155, 2023.

[6] L. C. Comandar et al., "Room temperature single-photon detectors for high bit rate quantum key distribution," *Appl. Phys. Lett.*, vol. 104, no. 2, 2014, Art. no. 021101.

[7] P. Keshavarzian et al., "A 3.3-Gb/s SPAD-based quantum random number generator," *IEEE J. Solid-State Circuits*, vol. 58, no. 9, pp. 2632–2647, Sep. 2023.

[8] J. Jin, T. Gerrits, and A. Gamouras, "Calibration and comparison of detection efficiency for free-space single-photon avalanche diodes at 850 nm," *Appl. Opt.*, vol. 61, no. 17, pp. 5244–5249, 2022.

[9] M. López et al., "A study to develop a robust method for measuring the detection efficiency of free-running InGaAs/InP single-photon detectors," *EPJ Quantum Technol.*, vol. 7, no. 1, 2020, Art. no. 14.

[10] L. Arabskyj et al., "Traceable characterisation of fibre-coupled single-photon detectors," *Metrologia*, vol. 61, no. 5, 2024, Art. no. 055008.

[11] B. Dejen, A. Vaquero-Stainer, T. Santana, L. Arabskyj, P. Dolan, and C. Chunnilall, "A refined method for characterizing afterpulse probability in single-photon avalanche diodes," *Appl. Phys. Lett.*, vol. 125, no. 19, 2024, Art. no. 194002.

[12] L. Arabskyj, B. Dejen, T. Santana, M. Lucamarini, C. Chunnilall, and P. Dolan, "Interference effects in commercially available free-space silicon single-photon avalanche diodes," *Appl. Phys. Lett.*, vol. 125, no. 19, 2024, Art. no. 194003.

[13] S. Virzí et al., "Detection efficiency characterization for free-space single-photon detectors: Measurement facility and wavelength-dependence investigation," *Appl. Phys. Lett.*, vol. 125, no. 22, 2024, Art. no. 221108.

[14] T. Gerrits et al., "Calibration of free-space and fiber-coupled single-photon detectors," *Metrologia*, vol. 57, no. 1, 2020, Art. no. 015002.

[15] M. López, H. Hofer, and S. Kück, "Detection efficiency calibration of single-photon silicon avalanche photodiodes traceable using double attenuator technique," *J. Modern Opt.*, vol. 62, no. 20, pp. 1732–1738, 2015.

[16] C. J. Chunnilall, I. P. Degiovanni, S. Kück, I. Müller, and A. G. Sinclair, "Metrology of single-photon sources and detectors: A review," *Opt. Eng.*, vol. 53, no. 8, 2014, Art. no. 081910.

[17] M. Stipčević, H. Skenderović, and D. Gracin, "Characterization of a novel avalanche photodiode for single photon detection in VIS-NIR range," *Opt. Exp.*, vol. 18, no. 16, pp. 17448–17459, 2010.

[18] F. Ceccarelli, G. Acconcia, A. Gulinatti, M. Ghioni, I. Rech, and R. Osellame, "Recent advances and future perspectives of single-photon avalanche diodes for quantum photonics applications," *Adv. Quantum Technol.*, vol. 4, no. 2, 2021, Art. no. 2000102.

[19] N. Gisin, G. Ribordy, W. Tittel, and H. Zbinden, "Quantum cryptography," *Rev. Modern Phys.*, vol. 74, pp. 145–195, 2002.

[20] M. Stipčević, D. Wang, and R. Ursin, "Characterization of a commercially available large area, high detection efficiency single-photon avalanche diode," *J. Lightw. Technol.*, vol. 31, no. 23, pp. 3591–3596, Dec. 2013.

[21] A. Lee, A. T. Castillo, C. Whitehill, and R. Donaldson, "The impact of spot-size on single-photon avalanche diode timing-jitter and quantum key distribution," *IET Quantum Commun.*, vol. 5, no. 4, pp. 443–449, 2024.

[22] A. Lee, R. Donaldson, C. Whitehill, and A. T. Castillo, "Multimode fiber influence on single-photon avalanche diode timing jitter," *Proc. SPIE*, vol. 12570, 2023, Art. no. 1257007.

[23] H. Mahmoudi, M. Hofbauer, B. Goll, and H. Zimmermann, "Noise and breakdown characterization of SPAD detectors with time-gated photon-counting operation," *Sensors*, vol. 21, no. 16, 2021, Art. no. 5287.

[24] J. Bienfang, T. Gerrits, P. Kuo, A. Migdall, S. Polyakov, and O. Slattery, "Single-photon sources and detectors dictionary," Nat. Inst. Standards Technol., Gaithersburg, MD, USA, NIST Interagency/Internal Rep. 8486, 2023. Accessed: Jun. 2025.

[25] A. Giudice et al., "High-rate photon counting and picosecond timing with silicon-SPAD based compact detector modules," *J. Modern Opt.*, vol. 54, no. 2–3, pp. 225–237, 2007.

[26] Z. Cheng, X. Zheng, D. Palubiak, M. J. Deen, and H. Peng, "A comprehensive and accurate analytical SPAD model for circuit simulation," *IEEE Trans. Electron Devices*, vol. 63, no. 5, pp. 1940–1948, May 2016.

[27] F. Guerrieri, S. Tisa, A. Tosi, and F. Zappa, "Two-dimensional SPAD imaging camera for photon counting," *IEEE Photon. J.*, vol. 2, no. 5, pp. 759–774, Oct. 2010.

[28] A. Giudici, G. Acconcia, I. Labanca, M. Ghioni, and I. Rech, "4 NS dead time with a fully integrated active quenching circuit driving a custom single photon avalanche diode," *Rev. Sci. Instrum.*, vol. 93, no. 4, 2022, Art. no. 043103.

[29] M. Stipčević, B. G. Christensen, P. G. Kwiat, and D. J. Gauthier, "Advanced active quenching circuit for ultra-fast quantum cryptography," *Opt. Exp.*, vol. 25, no. 18, pp. 21861–21876, 2017.

[30] A. Lacaita, S. Cova, M. Ghioni, and F. Zappa, "Single-photon avalanche diode with ultrafast pulse response free from slow tails," *IEEE Electron Device Lett.*, vol. 14, no. 7, pp. 360–362, Jul. 1993.

[31] M. Assanelli, A. Ingargiola, I. Rech, A. Gulinatti, and M. Ghioni, "Photon-timing jitter dependence on injection position in single-photon avalanche diodes," *IEEE J. Quantum Electron.*, vol. 47, no. 2, pp. 151–159, Feb. 2011.

[32] A. Lacaita, M. Mastrapasqua, M. Ghioni, and S. Vanoli, "Observation of avalanche propagation by multiplication assisted diffusion in p-n junctions," *Appl. Phys. Lett.*, vol. 57, no. 5, pp. 489–491, 1990.

[33] L. Li and L. M. Davis, "Single photon avalanche diode for single molecule detection," *Rev. Sci. Instrum.*, vol. 64, no. 6, pp. 1524–1529, 1993.

[34] A. Spinelli, L. M. Davis, and H. Dautet, "Actively quenched single-photon avalanche diode for high repetition rate time-gated photon counting," *Rev. Sci. Instrum.*, vol. 67, no. 1, pp. 55–61, 1996.

[35] I. Rech, I. Labanca, M. Ghioni, and S. Cova, "Modified single photon counting modules for optimal timing performance," *Rev. Sci. Instrum.*, vol. 77, no. 3, 2006, Art. no. 033104.

[36] H. Takesue, E. Diamanti, C. Langrock, M. M. Fejer, and Y. Yamamoto, "10-GHz clock differential phase shift quantum key distribution experiment," *Opt. Exp.*, vol. 14, no. 20, pp. 9522–9530, 2006.

[37] G. Kawata, J. Yoshida, K. Sasaki, and R. Hasegawa, "Probability distribution of after pulsing in passive-quenched single-photon avalanche diodes," *IEEE Trans. Nucl. Sci.*, vol. 64, no. 8, pp. 2386–2394, Aug. 2017.

[38] M. Hofbauer, K. Schneider-Hornstein, and H. Zimmermann, *Single-Photon Detection for Data Communication and Quantum Systems*. Bristol, U.K.: IOP Publishing, 2021.

[39] S. Cova, M. Ghioni, A. Lacaita, C. Samori, and F. Zappa, "Avalanche photodiodes and quenching circuits for single-photon detection," *Appl. Opt.*, vol. 35, no. 12, pp. 1956–1976, 1996.

[40] C. J. Chunnilall et al., "Calibration of free-space single-photon detectors," Forthcoming.

[41] J. S. Cheong, M. M. Hayat, X. Zhou, and J. P. R. David, "Relating the experimental ionization coefficients in semiconductors to the nonlocal ionization coefficients," *IEEE Trans. Electron Devices*, vol. 62, no. 6, pp. 1946–1952, Jun. 2015.

[42] "Excelitas technologies SPCM-AQRH-XX photon detection datasheet," *Rev. 2020-10*. 2020, Accessed: Jun. 2025. [Online]. Available: https://www.excelitas.com/sites/default/files/assets/product/document/24369.pdf

[43] "Excelitas technologies SPCM-AQRH-XX-TR photon detection datasheet," *Rev. 2020-04*. 2020, Accessed: Jun. 2025. [Online]. Avaiable: https://www.excelitas.com/product/spcm-aqrh-tr

[44] "Laser components COUNT-series user manual," V22. 2022, Accessed: Jun. 2025. [Online]. Available: https://www.lasercomponents.com/fileadmin/user_upload/home/Datasheets/manuals/lc-photon-counter/count-series-user-manual.pdf

[45] "Micro photon devices PDM series datasheet," 2025. Accessed: Dec. 2025. [Online]. Avaiable: https://www.micro-photon-devices.com/datasheet/MPD_PDM_Datasheet.pdf

[46] "Hamamatsu SPAD module C16531-100GD datasheet," No. KACC1312E05 2023-11. 2023, Accessed: Jun. 2025. [Online]. Available: https://www.hamamatsu.com/content/dam/hamamatsu-photonics/sites/documents/99_SALES_LIBRARY/ssd/c16531_series_kacc1312e.pdf

[47] "Laser components SAP-series silicon Geiger mode avalanche photodiode datasheet," V13 2023-01. 2023, Accessed: Jun. 2025. [Online]. Available: https://www.lasercomponents.com/fileadmin/user_upload/home/Datasheets/lc-apd/sap-series-geiger-mode-apd.pdf

[48] K. Dhoska, H. Hofer, B. Rodiek, M. López, T. Kübarsepp, and S. Kück, "Improvement of the detection efficiency calibration and homogeneity measurement of Si-SPAD detectors," *SpringerPlus*, vol. 5, no. 1, 2016, Art. no. 2065.